Boundary Extraction Based Imaging Method by Incorporating FDTD Based Wavefront Analysis for Microwave Mammography

Shouhei Kidera* and Kazuki Noritake†

Abstract — **Microwave UWB(Ultra Wideband) radar is promising as a non-invasive medical imaging, such as breast cancer or brain stroke detection due to its non-ionizing feature and deeper penetration ability in low loss medium. While various imaging algorithms has been developed, most of them are based on delay-and-sum (DAS) approach, which could not accurately reconstruct the boundary of dielectric object, even if a complete propagation model is given. This paper proposes a new scheme for accurate boundary extraction based on the range points migration (RPM) algorithm, where the candidate wavefront curve is accurately extracted by the FDTD based data generation. The results in numerical simulation assuming highly heterogeneous breast medium case, demonstrate that our algorithm achieves accurate boundary extraction for cancer shape estimation.**

1 introduction

Microwave mammography technique is one of the most promising alternative primary screening tools for X-ray based mammography, because it offers the potential for a low-cost, not painful, non-contact, and non-invasive modality in a non-ionizing range of the frequency spectrum. According to this background, various researches for microwave ultra-wideband (UWB) radar have been investigated, based on the physical basis on that there is distinguished contrast in the dielectric properties between normal and malignant tissues [1]. There are the literature, denoting that the structural characteristics of tumor can aid in distinguishing malignancies from benign lesions, and then accurate tumor-shape reconstruction has a potential to upgrade the microwave mammography screening tools, particularly for decreasing false-negative rate.

As a promising shape reconstruction scheme, there are two major approaches, one is the conformal approach, such as beam-forming [2] or time-reversal algorithms, and the other is based on the solution for the Helmholtz integral equation with linear or non-linear optimization scheme[3]. The conformal-based algorithm mainly relies on back-projective focusing for the recorded backscatters from the tumor, and requires accurate propagation model for penetrating dielectric medium, and suffers from insufficient spatial resolution or accuracy for object shape reconstruction even if the accurate propagation model is given. On the other hand, the inverse scattering algorithm based on the integral equation requires non-linear optimization schemes and suffers from an inaccuracy at the discontinuous gap with high-contrast dielectric object, such as gap between the normal and tumor tissues, and leads to the difficulty for accurate shape reconstruction of the malignant tumor.

To address with the above issue, this paper newly proposes the boundary extraction based imaging algorithm for object embedded in highly heterogeneous medium, e.g. breast media. This method is based on the principle of the range points migration (RPM) method [4, 5], where the accumulation degree of the intersection points between the multiple wavefronts is used for the reflection point reconstruction. Note that, the above wavefronts are extracted from the electric field map at the temporal snapshot accurately calculated by FDTD analysis, where the accurate propagation model is given. The numerical simulation using MRI-derived accurate breast phantom demonstrates that our proposed method accurately extracts the boundary gap between the tumor and adipose dominant tissue, even if highly heterogeneous distribution.

2 Observation model

We assume the measurement scenario for breast tumor imaging. The breast tissues are constituted of skin, adipose, fibroglandular and tumor, each of which has a lossy, dispersive and isotropic dielectric property. A set of transmitting and receiving antennas, located at (X, Y) is scanned along the circumference of breast media. $s'_{\rm bk}(X, Y, t)$ and $s'_{\rm tumor}(X, Y, t)$ is defined as the electric fields from background media (tumor is not included) and actual media (tumor is included), recorded at (X, Y) and time t. $s(X, Y, R)$ is defined as the output of matched filter applied to the signal $s'_{\rm tumor}(X, Y, t) - s'_{\rm bk}(X, Y, t)$, where $R = ct/2$ holds with the speed of light in air as c. The range point defined as $q \equiv (X, Y, R)$ is extracted from each local maxima of $s(X, Y, R)$. The conversion from each range point to its corresponding scattering center on tumor boundary is regarded as imaging in this context.

*Graduate School of Informatics and Engineering, The University of Electro-Communications, Japan, e-mail:kidera@uec.ac.jp

†Graduate School of Informatics and Engineering, The University of Electro-Communications, Japan,

978-1-5090-4451-1/17/$31.00

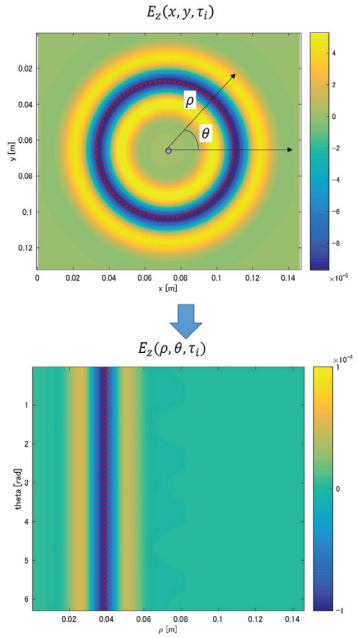

Figure 1: Conversion of electric field from $E(x, y, \tau_i)$ to $E(\rho, \theta, \tau_i)$ at the temporal snapshot $t = \tau_i$.

3 Proposed Boundary Extraction Method

3.1 Principle of RPM Imaging

The RPM imaging method is based on the conversion from the obtained range point to corresponding to the scattering center on object boundary. For this conversion, this method assesses the accumulation degrees of the intersection points of candidate curve, which is regarded as the wavefront reaching the object boundary. For the specific range point as $\boldsymbol{q}_i = (X_i, Y_i, R_i)$, the scattering center is calculated as;

$$\hat{\boldsymbol{p}}(\boldsymbol{q}_i) = \underset{\boldsymbol{p}^{\mathrm{int}}(\boldsymbol{q}_i;\boldsymbol{q}_j)}{\arg\max} \sum_k g(\boldsymbol{q}_i; \boldsymbol{q}_j, \boldsymbol{q}_k) \times \exp\left\{ -\frac{\|\boldsymbol{p}^{\mathrm{int}}(\boldsymbol{q}_{\mathrm{i}}; \boldsymbol{q}_{\mathrm{j}}) - \boldsymbol{p}^{\mathrm{int}}(\boldsymbol{q}_{\mathrm{i}}; \boldsymbol{q}_{\mathrm{k}})\|^2}{2\sigma_r^2} \right\} \quad (1)$$

where σ_r is empirically determined constant, and

$$g(\boldsymbol{q}_i; \boldsymbol{q}_j, \boldsymbol{q}_k) = s(\boldsymbol{q}_j)\exp\left\{ -\frac{D(\boldsymbol{q}_i, \boldsymbol{q}_j)^2}{2\sigma_D^2} \right\} + s(\boldsymbol{q}_k)\exp\left\{ -\frac{D(\boldsymbol{q}_i, \boldsymbol{q}_k)^2}{2\sigma_D^2} \right\} \quad (2)$$

where $D(\boldsymbol{q}_i, \boldsymbol{q}_j) \equiv \sqrt{(X_i - X_j)^2 + (Y_i - Y_j)^2}$ holds and σ_D denotes the empirically determined constant Note that $\boldsymbol{p}^{\mathrm{int}}(\boldsymbol{q}_i; \boldsymbol{q}_j)$ denotes the intersection point of the wavefronts. However, these wavefronts are hardly obtained in the case that the background medium propagation model is not given.

3.2 FDTD-based wavefront

The specific methodology is described as follows. In the monostatic case, the above wavefront can be calculated by the spatial distribution of electric field snapshot at the time $\tau_i = R_i/c$ at i-th range point (X_i, Y_i, R_i), because the forward and backward propagation path should be same in this observation. Then, if the complete information of background medium dielectric property is given, such wavefront can be accurately calculated by FDTD method. To obtain the FDTD based wavefront, we convert the electric field $E(x, y, \tau_i)$ to $E(\rho, \theta, \tau_i)$, where $\rho = \sqrt{(x - X_i)^2 + (t - Y_i)^2}$ and $\theta = \tan^{-1}\left(\frac{y - Y_i}{x - X_i}\right)$. Figure 1 shows the example of the conversion of electric field. After the conversion, we extract the maximum peaks of $E(\rho, \theta, \tau_i)$ as to each θ, and their corresponding ρ is defined as $\rho_i(\theta)$. Then, the wavefront curve $F_i(X, i, Y_i)$ for each range point (X_i, Y_i, R_i) is denoted as

$$\boldsymbol{F}_i(\theta) = (X_i, Y_i) + \rho_i(\cos\theta, \sin\theta), (0 \leq \theta \leq 2\pi), \quad (3)$$

After this step, the intersection points between the curves $\boldsymbol{F}_i(\theta)$ and $\boldsymbol{F}_j(\theta)$ can be determined as $\boldsymbol{p}^{\mathrm{int}}(\boldsymbol{q}_i; \boldsymbol{q}_j)$. By using this process, the RPM based boundary extraction is achieved in this situation.

4 Numerical Simulation Examples

4.1 Breast phantom model

We test the two types of realistic breast phantoms derived from MRIs of healthy women [**?**] are investigated; Class 3 as "heterogeneously dense" phantom (ID number 062204). which are available from online University of Wisconsin repository [6]). The frequency-dependent complex permittivities for skin and breast tissues in the phantoms modeled by single-pole Debye models over the frequency range of 0.1-5 GHz are referred from. Figure 2 illustrates the actual dielectric property maps of "Class 3", including large-scale tumor as the static conductivity and $\Delta\epsilon$, which denotes the difference of relative permittivities from infinite frequency to zero frequency. Circular shaped high-contrast object modeling malignant tumor is embedded in this heterogeneous breast medium. The mono-static radar is scanned along the circumference surrounding the breast with 36 sample points. The transmitting signal forms the Gaussian modulated pulse, whose center frequency is 2.45 GHz with 1.9 GHz frequency bandwidth. The received data are generated through FDTD, where the spatial grid size is 0.5 mm. The FDTD generates the single-pole Debye dispersive data, where the relaxation time 15 psec is used for all tissues, for simplicity.

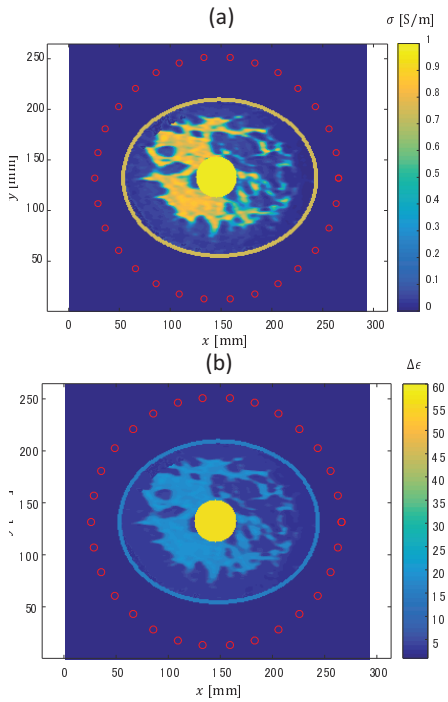

Figure 2: The dielectric map of breast media and large-shape tumor. (a): Conductivity and (b): $\Delta\epsilon$, where red hollow circles denote the observation points in monostatic observation.

4.2 Results

At first, for the method comparison, the DAS based method is investigated. Note that, in this case, the the FDTD based calculated electric field at the appropriate snapshot is synthesized, namely, the complete propagation model is given to DAS process. Figure 3 shows the result of DAS image, and it shows that while the image focuses on the area around the tumor, its boundary is considerably blurred because it assumes point-wise shape focusing scheme. This result shows that even if we obtain infinite SCR and complete propagation path, the DAS based method could not reconstruct the distinguished boundary, which denotes the upper limitation of DAS performance.

Next, we show the performance of RPM based proposed method as follows. Figure 4 shows the two examples of the snapshot of electric field $E(\rho, \theta, \tau_i)$ at different sensor locations, and their extracted wavefronts. As shown in this figure, the FDTD based calculated wavefront could reach the actual tumor boundary. Finally, we show the RPM image in Fig. **??**. This figure clearly shows that the RPM based method accurately determines each boundary point converted from the observed time delay (range point), which enables us to assess the shape of tumor, appropriately. The calculation time for reconstruction is within 10 min using Intel Core

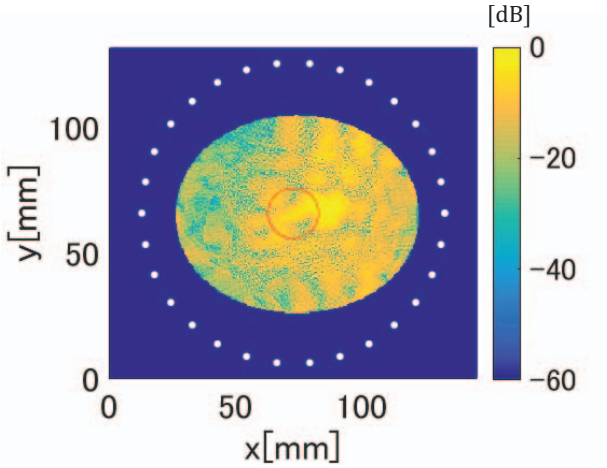

Figure 3: DAS image, when the complete propagation path is given.

i5 CPU 3.3 GHz, with 8 GB RAM. The main part of the computational cost is that of FDTD, but this level of computational cost is not serious in the actual medical imaging scene.

5 Conclusion

This paper proposed accurate boundary reconstruction method based on the RPM algorithm and FDTD based wavefront extraction. The numerical example, assuming realistic MRI-derived breast phantom, demonstrates that the proposed method achieves remarkably accurate boundary reconstruction, which is overwhelmed by the limitation of DAS based imaging scheme. Note that, the proposed method is based on the assumption that the response from background media is completely removed, and the dielectric property of background media is completely given. We consider that such information is in actual screening test, if the time differential observation for subject is available, and time evolution of tumor could be monitored by this algorithm.

Acknowledgment

This research and development work was supported by the MIC/SCOPE #162103102. We use the dispersive FDTD code developed in the Cross-Disciplinary Laboratory in University of Wisconsin-Madison, lead by Prof. Susan C. Hagness.

References

[1] A. J. Surowiec, S. S. Stuchly, J. R. Barr, and A. Swarup, "Dielectric properties of breast carcinoma and the surrounding tissues," *IEEE*

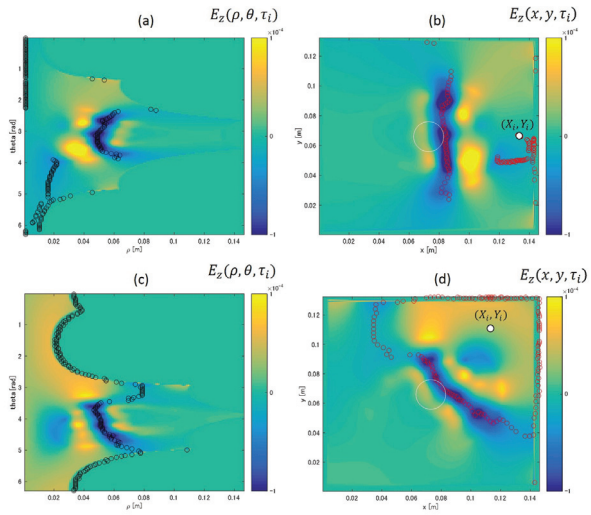

Figure 4: Two examples of the snapshot of electric fields $E(\rho, \theta, \tau_i)$ at different sensor locations (X_i, Y_i). (a) and (c) denote $E(\rho, \theta, \tau_i)$ and (b) and (d) denote $E(x, y, \tau_i)$ and extracted wavefronts (red solid circles) for each observation point.

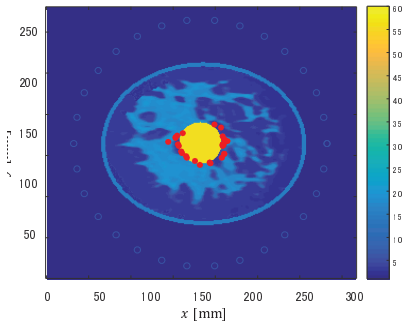

Figure 5: Reconstructed boundary points obtained by the proposed method.

Trans.Biomed. Eng., vol. BME-35, pp. 257–263, Apr. 1988.

[2] E. J. Bond, *et al*, "Microwave imaging via space-time beamforming for early detection of breast cancer", *IEEE Trans. Antennas Propagat.*, vol. 1, no. 8, pp. 1690-1705, Aug. 2003.

[3] A. Franchois and C. Pichot, "Microwave Imaging-Complex Permittivity Reconstruction with a Levenberg-Marquardt Method," *IEEE Trans. Antennas Propagat.*, vol. 45, no. 2, pp. 203–215, Feb., 1997.

[4] S. Kidera, T. Sakamoto and T. Sato, "Accurate UWB Radar 3-D Imaging Algorithm for Complex Boundary without Range Points Connections", IEEE Trans. Geoscience and Remote Sensing, vol.48, no. 4, pp. 1993–2004, Apr., 2010.

[5] K. Akune, S. Kidera and T. Kirimoto, "Accurate and Nonparametric Imaging Algorithm for Targets Buried in Dielectric Medium for UWB Radars", *IEICE Trans. Electronics*.,vol. E95-C, no. 8, pp. 1389-1398, Aug., 2012.

[6] University of Wisconsin Cross-Disciplinary Electromagnetics Laboratory (UWCEM), gNumerical breast phantom repositoryh [Online]. Available: http://uwcem.ece.wisc.edu, accessed on: Feb. 10, 2016.